



# Spectroscopy of Ethylenedione\*\*

Andrew R. Dixon, Tian Xue, and Andrei Sanov\*

**Abstract:** The long sought-after, intrinsically short-lived molecule ethylenedione (OCCO) was observed and investigated by anion photoelectron spectroscopy. The adiabatic electron affinity of its quasi-bound  $^3\Sigma_g^-$  state is 1.936(8) eV. The vibrational progression with a 417(15)  $\text{cm}^{-1}$  frequency observed within the triplet band corresponds to a trans-bending mode. Several dissociative singlet states are also observed, corresponding to two components of the  $^1\Delta_g$  state and the  $^1\Sigma_g^+$  state. The experimental results are in agreement with theoretical predictions and constitute the first spectroscopic observation and characterization of this elusive compound.

We report a spectroscopic characterization of ethylenedione (OCCO). This report follows a century-long history of controversy and failed attempts to observe this deceptively simple molecule.<sup>[1]</sup> It began in 1913, when the reaction of oxalyl bromide with mercury to form CO was postulated to include an “OC:CO” intermediate.<sup>[2]</sup> In the 1940s, “O=C=C=O” was claimed to be the active component of Glyoxylide, a purported antidote for a long list of afflictions, from exhaustion to cancer. However, the reports and the wonder drug itself were classified as fraud by the U.S. Food and Drug Administration.<sup>[3]</sup>

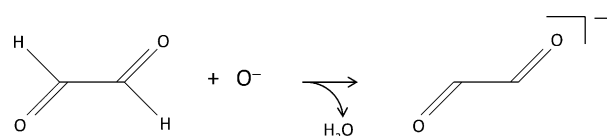
For decades, OCCO has continued to be pursued as a synthetic target,<sup>[4–7]</sup> but all past studies<sup>[1,4,7–9]</sup> failed to provide conclusive evidence of the existence of this “exceedingly coy molecule”.<sup>[1]</sup> To this day, OCCO has remained unobserved, not only as a substance, but even as a transient species. Its mysteriously elusive nature conflicts with the convincing theoretical evidence of a stable covalent OCCO minimum on the  $\text{C}_2\text{O}_2$  potential energy surface.<sup>[7,10,11]</sup> To deepen the controversy, the sulfur and selenium analogues OCCS, SCCS, and SeCCSe have all been observed and studied experimentally,<sup>[12–14]</sup> but not OCCO.

Despite the straightforward closed-shell Kekulé structure ( $\text{O}=\text{C}=\text{C}=\text{O}$ ), the lowest bound state of OCCO is a linear triplet, with the unpaired electrons occupying two degenerate  $\pi$  orbitals.<sup>[1,10,11,15,16]</sup> This motif puts OCCO in the same class as  $\text{O}_2$ . Although the triplet is bound, it is theorized to cross to the nearby singlet, which in turn dissociates rapidly to two CO molecules.<sup>[7,10,17]</sup> This process is exothermic by several electron volts,<sup>[10,11]</sup> hence the unstable nature of the molecule.

However, the triplet–singlet crossing is predicted to occur on a nanosecond timescale,<sup>[7]</sup> making triplet OCCO a spectroscopically long-lived species with no good reason to evade detection.

It is against this backdrop that we report the direct spectroscopic observation and characterization of OCCO. Forgoing strategies based on the neutral species, we accessed its low-lying states by the photodetachment of the stable anion,  $\text{OCCO}^-$ .<sup>[18,19]</sup> The photoelectron spectra are in excellent agreement with theory, reinforcing the conclusion that the observed states belong to OCCO. Although the equilibrium structure of the anion corresponds to a *trans*-bent  $\text{C}_{2h}$  geometry,<sup>[18,19]</sup> the relaxed vibrational state of linear ethylenedione is accessed in the experiment.

We synthesized the anion by the  $\text{H}_2^+$  abstraction reaction of  $\text{O}^-$  with glyoxal:<sup>[20,21]</sup>



The reaction was performed in an electron-impact-ionized supersonic expansion. The photoelectron spectra were collected using a previously described imaging apparatus.<sup>[22]</sup>

The photoelectron spectrum of  $\text{OCCO}^-$  at 532 nm is presented in Figure 1 A. It consists of a vibrational progression ( $T_0$ ) on top of a broad pedestal ( $S_1$ ). The spectral structure suggests the involvement of two types of neutral states: a long-lived state that gives rise to the progression and another state that is responsible for the pedestal. The latter may be dissociative or involve a large geometry change relative to the anion. Another indication of two electronic transitions is based on the photoelectron anisotropy parameter ( $\beta$ ).<sup>[23]</sup> The  $\beta$  values for the  $T_0$  peaks are shown in Figure 1 A as open circles, whereas the average for the  $S_1$  tail is displayed as a filled circle. The discontinuity between the filled and open symbols, observed despite the overlap between the bands, suggests that they correspond to different transitions.

Based on these (thus far) qualitative observations, we assigned the progression in Figure 1 A to the bound triplet state of OCCO, which is consistent with its expected (sub-) nanosecond lifetime,<sup>[7]</sup> whereas the broad pedestal was assigned to a dissociative singlet. The following quantitative analysis supports these assignments. The adiabatic electron affinity (EA) of triplet ethylenedione was determined to be  $\text{EA} = 1.936(8) \text{ eV}$  based on the first  $T_0$  peak. The  $T_0$  progression is consistent with the geometry difference between the anion and the linear OCCO triplet. The average spacing of 417(15)  $\text{cm}^{-1}$  is close to the 396  $\text{cm}^{-1}$  frequency of

[\*] A. R. Dixon, T. Xue, Prof. Dr. A. Sanov  
Department of Chemistry and Biochemistry  
University of Arizona  
Tucson, AZ 85721-0041 (USA)  
E-mail: sanov@u.arizona.edu

[\*\*] We thank Dr. Dmitry Khuseynov for his encouragement at the early stage of the project. William P. Brezinski and Richard F. Vreeland are acknowledged for their help with dehydration of the glyoxal precursor. This work was supported by the U.S. National Science Foundation (CHE-1266152).

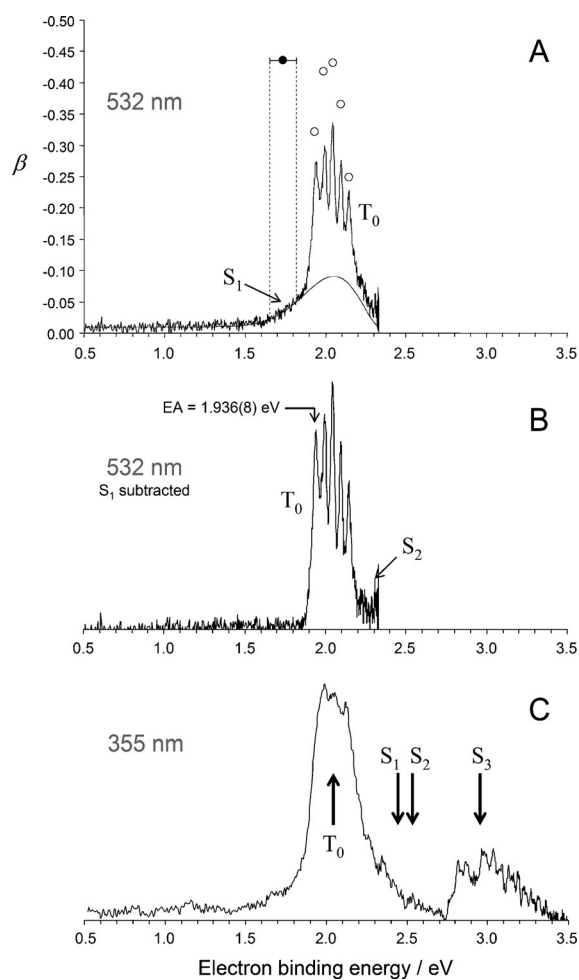


**Figure 1.** A) Photoelectron spectrum of  $\text{OCCO}^-$  at 532 nm;  $\circ$ : the photoelectron anisotropy parameter  $\beta$  for the peaks of the  $T_0$  progression;  $\bullet$ : the same parameter for the  $S_1$  tail, with the dotted lines indicating the energy range. Gray curve: simulation of the  $S_1$  band. B) The above spectrum with the  $S_1$  model band subtracted. C) The 355 nm spectrum. Vertical arrows indicate the VDEs corresponding to the neutral states, based on the calculations presented in Figure 2 B.

the *trans*-bending mode of  $^3\Sigma_g^- \text{OCCO}$ , as predicted by MCSCF/cc-pVTZ calculations.<sup>[10]</sup> The  $S_1$  pedestal extends lower in energy than the triplet EA value owing to the dissociative nature of the singlet. The adiabatic minimum of the singlet surface corresponds to the  $\text{CO}(^1\Sigma^+) + \text{CO}(^1\Sigma^+)$  limit, some 2.55 eV below the triplet equilibrium.<sup>[19]</sup> The dissociation limit has no measurable Franck–Condon overlap with the  $\text{OCCO}^-$  anion, but the  $S_1$  tail in Figure 1 A reflects the downhill structure of the singlet surface.

Neutral  $\text{OCCO}$  and its anion have been the subjects of many theoretical studies.<sup>[7,10,11,19]</sup> The relevant states involve two nearly degenerate orbitals,  $6b_u$  and  $2a_u$  (at a  $C_{2h}$  geometry), which are shown schematically in Figure 2 A. At linearity, they turn into the degenerate  $2\pi_u$  orbitals, and their population with two electrons gives rise to the  $^3\Sigma_g^-, ^1\Delta_g$ , and  $^1\Sigma_g^+$  states of  $\text{OCCO}$ , as indicated in Figure 2 B (right). The energy gaps shown are from the MRCI/cc-pVTZ//B3LYP/6-311 + G(2df) calculations by Talbi and Chandler.<sup>[10]</sup> Whereas the singlets dissociate to  $2\text{CO}(^1\Sigma^+)$ , this channel is inacces-

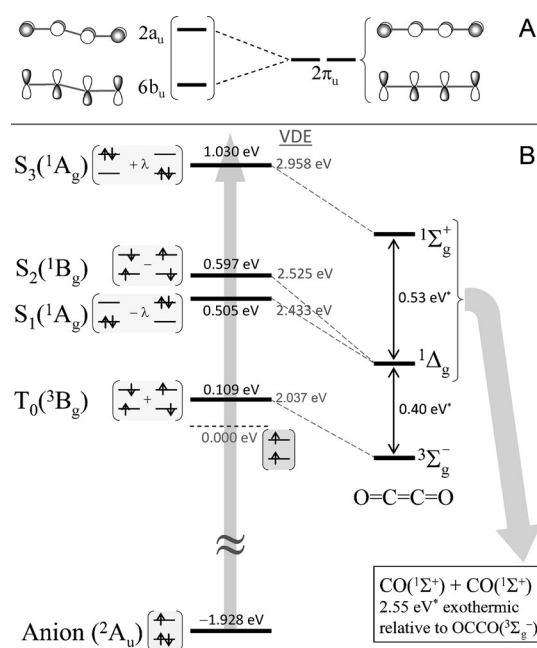


**Figure 2.** A) Left: The  $6b_u$  and  $2a_u$  orbitals of  $\text{OCCO}^-$  at the anion geometry. Right: Degenerate  $2\pi_u$  linear-geometry orbitals that correlate to  $6b_u$  and  $2a_u$ . B) Left: labels, dominant configurations, and energy levels of the  $\text{OCCO}^-$  and  $\text{OCCO}$  states at the anion geometry. The electron configurations are abbreviated in terms of the  $6b_u$  and  $2a_u$  orbitals. All properties were determined by EOM-IP/SF-CCSD/aug-cc-pVTZ calculations for the  $\text{OCCO}^-$  geometry optimized at the CCSD/aug-cc-pVTZ level of theory. The zero of energy corresponds to the  $M_s = 1$   $^3B_g$  reference. The values shown alongside the states are the VDEs. Right: Schematic representation of the energetics of linear  $\text{OCCO}$ . The vertical gaps (\*) were taken from Ref. [10].

sible on the triplet surface. All other dissociation channels are significantly higher in energy.

To complement the experimental results, we carried out calculations specifically targeting  $\text{OCCO}^-$  photodetachment. To meet the needs of these calculations, the anion geometry was optimized<sup>[24]</sup> at the CCSD level with the aug-cc-pVTZ basis set. In accord with past studies,<sup>[19]</sup> this yielded an  $\text{OCCO}^-$  structure of  $C_{2h}$  symmetry, with C=O and C=C bond lengths of 1.240 and 1.281 Å, respectively, and a C-C-O angle of 161.2°. This geometry was used for the calculations employing the equation of motion (EOM) ionization potential (IP) and spin flip (SF) methods,<sup>[25]</sup> combined with coupled cluster theory, using Q-Chem 4.0.<sup>[26]</sup> This method was used to describe the multi-configurational nature of the  $\text{OCCO}$  diradical states.

First, the vertical detachment transitions at the anion geometry were explored with the EOM-IP-CCSD method. The neutral states were accessed from the  $^2A_u: \dots(6b_u)^2(1a_u)^1$  reference. Removal of the beta-spin  $6b_u$  electron results in the high-spin ( $M_s = 1$ )  $^3B_g: \dots(6b_u)^1(1a_u)^1$  configuration, which is indicated in Figure 2 B. The corresponding excitation energy of 1.928 eV will be used in what follows as the estimated gap between the anion and the high-spin triplet reference.

Second, EOM-SF-CCSD calculations were performed for the same anion geometry, using the high-spin triplet reference. Combinations of one-electron SF excitations yielded the

low-spin ( $M_s=0$ ) component of the  $T_0(^3B_g)$  state and three singlet states ( $S_1$ ,  $S_2$ , and  $S_3$ ). The  $T_0(^3B_g)$  energy in Figure 2B corresponds to the low-spin ( $M_s=0$ ) component, as recommended by Krylov and Slipchenko.<sup>[27]</sup> The dominant configurations and state energies relative to the triplet reference are also shown.

Combining the IP energy for the anion with the SF energies of the neutral compounds, the vertical detachment energies (VDEs) corresponding to different OCCO states were determined and are given in Figure 2B. The predicted VDE of 2.037 eV for the  $T_0$  transition is in excellent agreement with the most intense peak in Figure 1A. The first singlet state  $S_1(^1A_g)$  corresponds to a theoretical VDE of 2.433 eV, which is slightly above the 532 nm photon energy used to collect the data in Figure 1A. This state dissociates to  $CO(^1\Sigma^+) + CO(^1\Sigma^+)$ , and although it lies above  $T_0$  at the anion geometry, its adiabatic minimum is much lower in energy than the  $T_0$  equilibrium. The down-slope shape of the potential manifests as the low-energy  $S_1$  tail in Figure 1A, extending below the  $T_0$  origin.

The calculated VDE allows us to model the  $S_1$  band, as shown by the gray curve in Figure 1A. The simulation assumes a Gaussian envelope centered at  $VDE=2.433$  eV. To account for the photon-energy cut-off and the electron kinetic energy dependence of the cross-section, the envelope was scaled with a Wigner-like<sup>[28]</sup> pre-factor assuming an (intermediate)  $3/2$  effective exponent.<sup>[29]</sup> Subtracting the model curve from the experimental data yielded the spectrum in Figure 1B, clearly showing the  $T_0$  progression with the origin at  $EA=1.936(8)$  eV and the most intense peak at  $VDE=2.04(2)$  eV. Aside from the  $T_0$  band, the spectrum in Figure 1B shows an additional signal  $S_2$  near the photon-energy cut-off. Although this assignment is not definitive, we attribute this extra signal to the  $S_2(^1B_g)$  state, predicted to lie slightly above  $S_1$ , at a VDE of 2.525 eV (see Figure 2B).

Figure 1C shows another spectrum, which was collected at 355 nm. Despite its lower resolution, the  $T_0$  peak indeed shows the low- and high-energy shoulders attributed to the  $S_1$  and  $S_2$  states. The spectrum shows an additional band ( $S_3$ ), whose position is in agreement with the VDE predicted for the  $^1A_g$  state. The vertical arrows in Figure 1C indicate the VDEs corresponding to all four neutral states, taken from the results in Figure 2B. The 355 nm spectrum is completely consistent with the predicted properties of OCCO, just like the 532 nm spectrum.

In conclusion, the reported spectra reflect the low-lying electronic states of the elusive OCCO molecule. The electron affinity of the quasi-bound  $^3\Sigma_g^-$  state is 1.936(8) eV, whereas the vertical detachment energy of the  $OCCO^-$  anion is 2.04(2) eV. Three singlet neutral states were also observed. The results are in excellent agreement with the predictions of theory and constitute the first spectroscopic observation of ethylenedione. This work paves the way for time-resolved studies of transient OCCO by means of charge-reversal spectroscopy.<sup>[30]</sup> The photodetachment of  $OCCO^-$ , as described here, launches dynamics on the neutral surface(s), with a predicted lifetime of approximately 0.5 ns for the triplet.<sup>[7]</sup> These dynamics and the appearance of the  $CO(^1\Sigma^+)$  products can be probed by delayed photoionization.

## Experimental Section

The refrigerated glyoxal precursor (40 % w/w, aq) was dried over 3 Å molecular sieves for 24 h and then decanted. The dried solution was placed in a sample holder connected to the carrier gas line and mildly heated to increase the vapor pressure. The reaction of glyoxal with  $O^-$  was performed in an electron-impact-ionized supersonic expansion of the precursor vapor seeded in  $N_2O$ . The anions with  $M_w=56$  were photodetached using the second (532 nm) or third (355 nm) harmonics of a neodymium:yttrium aluminum garnet laser. The photoelectron images were analyzed following published procedures.<sup>[22,31]</sup>

**Keywords:** anions · diradicals · electronic structure · photoelectron spectroscopy · transient molecules

**How to cite:** *Angew. Chem. Int. Ed.* **2015**, *54*, 8764–8767  
*Angew. Chem.* **2015**, *127*, 8888–8891

- [1] E. G. Lewars in *Modeling Marvels*, Springer, Berlin, **2008**, p. 131.
- [2] H. Staudinger, E. Anthes, *Ber. Dtsch. Chem. Ges.* **1913**, *46*, 1426.
- [3] W. W. Goodrich, *History of the U. S. Food and Drug Administration* (interview by R. T. Ottens and F. L. Lofsvold), Food and Drug Administration History Office, Rockville, Maryland, **1986**, <http://www.fda.gov/downloads/aboutfda/whatwedo/history/oralhistories/selectedoralhistorytranscripts/ucm372999.pdf>.
- [4] J. A. Berson, D. M. Birney, W. P. Dailey, J. F. Liebman in *Modern Models of Bonding and Delocalization, Molecular Structures and Energetics*, Vol. 6 (Eds.: J. F. Liebman, A. Greenberg), VCH, Weinheim, **1988**, p. 391.
- [5] M. B. Rubin, A. Patyk, W. Sander, *Tetrahedron Lett.* **1988**, *29*, 6641.
- [6] D. Sülzle, T. Weiske, H. Schwarz, *Int. J. Mass Spectrom. Ion Processes* **1993**, *125*, 75.
- [7] D. Schröder, C. Heinemann, H. Schwarz, J. N. Harvey, S. Dua, S. J. Blanksby, J. H. Bowie, *Chem. Eur. J.* **1998**, *4*, 2550.
- [8] L. A. Surin, D. N. Fourzikov, F. Lewen, B. S. Dumes, G. Winnewisser, A. R. W. McKellar, *J. Mol. Spectrosc.* **2003**, *222*, 93.
- [9] H. W. Chen, J. L. Holmes, *Int. J. Mass Spectrom. Ion Processes* **1994**, *133*, 111.
- [10] D. Talbi, G. S. Chandler, *J. Phys. Chem. A* **2000**, *104*, 5872.
- [11] C. Trindle, *Int. J. Quantum Chem.* **2003**, *93*, 286.
- [12] D. Sülzle, J. K. Terlouw, H. Schwarz, *J. Am. Chem. Soc.* **1990**, *112*, 628.
- [13] C. T. Pedersen, M. W. Wong, K. Takimiya, P. Gerbaux, R. Flammang, *Aust. J. Chem.* **2014**, *67*, 1195.
- [14] G. Maier, H. P. Reisenauer, R. Ruppel, *Angew. Chem. Int. Ed. Engl.* **1997**, *36*, 1862; *Angew. Chem.* **1997**, *109*, 1972.
- [15] G. P. Raine, H. F. Schaefer, R. C. Haddon, *J. Am. Chem. Soc.* **1983**, *105*, 194.
- [16] N. L. Ma, M. W. Wong, *Angew. Chem. Int. Ed.* **1998**, *37*, 3402; *Angew. Chem.* **1998**, *110*, 3587.
- [17] A. A. Korkin, A. Balkova, R. J. Bartlett, R. J. Boyd, P. V. Schleyer, *J. Phys. Chem.* **1996**, *100*, 5702.
- [18] W. E. Thompson, M. E. Jacox, *J. Chem. Phys.* **1991**, *95*, 735.
- [19] J. R. Thomas, B. J. DeLeeuw, P. O'Leary, H. F. Schaefer, B. J. Duke, B. O'Leary, *J. Chem. Phys.* **1995**, *102*, 6525.
- [20] J. Lee, J. J. Grabowski, *Chem. Rev.* **1992**, *92*, 1611.
- [21] J. J. Grabowski, S. J. Melly, *Int. J. Mass Spectrom. Ion Processes* **1987**, *81*, 147.
- [22] L. Velarde, T. Habteyes, A. Sanov, *J. Chem. Phys.* **2006**, *125*, 114303.
- [23] A. Sanov, *Annu. Rev. Phys. Chem.* **2014**, *65*, 341.
- [24] M. J. Frisch et al., Revision A.1, Gaussian, Inc., Wallingford, CT, **2009**.
- [25] A. I. Krylov, *Annu. Rev. Phys. Chem.* **2008**, *59*, 433.
- [26] Y. Shao et al., *Phys. Chem. Chem. Phys.* **2006**, *8*, 3172.

- [27] L. V. Slipchenko, A. I. Krylov, *J. Chem. Phys.* **2002**, *117*, 4694.  
 [28] E. P. Wigner, *Phys. Rev.* **1948**, *73*, 1002.  
 [29] D. Khuseynov, A. R. Dixon, D. J. Goebbert, A. Sanov, *J. Phys. Chem. A* **2013**, *117*, 10681.  
 [30] D. W. Boo, Y. Ozaki, L. H. Andersen, W. C. Lineberger, *J. Phys. Chem. A* **1997**, *101*, 6688.  
 [31] V. Dribinski, A. Ossadtchi, V. A. Mandelshtam, H. Reisler, *Rev. Sci. Instrum.* **2002**, *73*, 2634.

Received: April 15, 2015  
 Published online: June 18, 2015